

# Highly variable carbon environment in the $\kappa$ -(BEDT-TTF)<sub>2</sub>Cu<sub>2</sub>(CN)<sub>3</sub> salt probed by carbon *K*-edge x-ray absorption and resonant inelastic x-ray scattering spectroscopy

Djénabou Bayo <sup>1,2,3</sup>, Victor Balédent <sup>4</sup>, Alberto Boccuni,<sup>1</sup> Vita Ilakovac,<sup>1,5,\*</sup> Stéphane Carniato,<sup>1</sup> Pascale Foury-Leylekian <sup>4</sup>, Jean-Paul Pouget,<sup>4</sup> Alessandro Nicolaou <sup>6</sup>, Kari Ruotsalainen <sup>7</sup>, Azzedine Bendouan <sup>6</sup>, Meryem Bouaziz,<sup>6</sup> Yves Joly <sup>8</sup>, Kazuya Miyagawa <sup>9</sup>, Kazushi Kanoda <sup>9</sup> and Silvia Tomić <sup>10</sup>

<sup>1</sup>*Sorbonne Université, CNRS, LCPMR, F-75252 Paris, France*

<sup>2</sup>*Department of Physics, University of Warwick, Coventry CV4 7AL, United Kingdom*

<sup>3</sup>*LPTM, CNRS UMR 8089, CY Cergy-Paris Université, Cergy-Pontoise, France*

<sup>4</sup>*LPS, CNRS UMR 8502, Université Paris Saclay, Orsay, France*

<sup>5</sup>*CY Cergy-Paris Université, F-95031 Cergy-Pontoise, France*

<sup>6</sup>*Synchrotron SOLEIL, B.P. 48, F-91192 Gif-sur-Yvette, France*

<sup>7</sup>*European Synchrotron Radiation Facility, 71 Avenue des Martyrs, Grenoble 38000, France*

<sup>8</sup>*Université Grenoble Alpes, CNRS, Institut Néel, 38042 Grenoble, France*

<sup>9</sup>*Department of Applied Physics, University of Tokyo, Tokyo 113-8656, Japan*

<sup>10</sup>*Insititut za Fiziku, Bijenička c. 46, HR-10000 Zagreb, Croatia*



(Received 21 November 2024; revised 9 February 2025; accepted 26 February 2025; published 27 March 2025)

Using near-edge x-ray absorption fine structure (NEXAFS) and resonant inelastic x-ray scattering (RIXS) at the C *K*-edge, we have studied the carbon environment and dynamics in  $\kappa$ -(BEDT-TTF)<sub>2</sub>Cu<sub>2</sub>(CN)<sub>3</sub> and supplemented them by density functional theory calculations. The maximum in the NEXAFS pre-edge is identified to originate mainly from nonequivalent carbon sites of the BEDT-TTF molecule, whereas the anionic carbons contribute to the intensity at higher energy. RIXS spectra show resonant reinforcement of the interorbital excitations, but without a clear set of vibrational harmonics, previously detected in our N *K*-edge RIXS study. This finding points to the strong multimode vibrational excitation of all carbon sites in both (BEDT-TTF)<sub>2</sub><sup>+</sup> molecular and Cu<sub>2</sub>(CN)<sub>3</sub><sup>-</sup> anionic subsystems, thus demonstrating a strongly disordered environment which might have important implications for the electronic state of the  $\kappa$ -(BEDT-TTF)<sub>2</sub>Cu<sub>2</sub>(CN)<sub>3</sub>.

DOI: [10.1103/PhysRevB.111.125160](https://doi.org/10.1103/PhysRevB.111.125160)

## I. INTRODUCTION

The quasi-two-dimensional organic charge-transfer salts belong to a vast class of strongly correlated materials which exhibit some of the most intriguing phenomena in condensed matter physics [1]. Among them,  $\kappa$ -(BEDT-TTF)<sub>2</sub>X, where BEDT-TTF (shortly, ET) is bis(ethyl enedithio) tetrathiafulvalene (Fig. 1) and X is a monovalent counterion, have attracted much attention for their variety of electronic states due to the interplay of reduced dimensionality, strongly correlated electrons, spin-charge interactions, and ordering phenomena. Most prominent is  $\kappa$ -(BEDT-TTF)<sub>2</sub>Cu<sub>2</sub>(CN)<sub>3</sub> (shortly,  $\kappa$ -Cu), which has gained wide attention in the solid-state community since it was synthesized in 1991 [2]. It possesses a rich phase diagram under pressure, featuring a Mott metal-insulator transition, unconventional superconductivity, and non-Fermi-liquid behavior [3–5]. Furthermore, it is extensively discussed as a prime candidate for hosting a quantum spin liquid (QSL) consisting of entangled spin singlets with exotic low-energy excitations [6,7].

The  $\kappa$ -Cu structure is composed of conducting layers of organic ET molecules, which are separated by nonconducting anion planes parallel to the (*b,c*) crystallographic plane (Fig. 2). The anion layer consists of an essentially planar polymeric network of triangularly coordinated copper (I) ions interconnected by cyanide (CN) groups [2]. The connection of the molecular and the anion layers is realized via hydrogen H bonds between molecular-layer ending ethylene groups and anion-layer CN groups. There is a charge transfer of about one electron per dimer, from the ET molecular layer (donor) to the anion plane (acceptor). The sites of the triangular lattice of ET dimers are accommodated by approximately one hole carrying a spin-1/2. Commonly, anions were considered to serve as the spacer and charge reservoir, until the important role of ET molecule-anion interaction in stabilization of diverse electronic phases was emphasized [8].

At ambient pressure,  $\kappa$ -Cu is a Mott insulator with correlation strength  $U/W \approx 1$  ( $U$  is the on-site Coulomb repulsion and  $W$  is the bandwidth), implying that it lies close to the metal-to-insulator transition. At high temperatures, DC electrical transport takes place by the nearest-neighbor hopping of holes within molecular planes, whereas below 130 K, DC conduction crosses over to the variable-range hopping [9]. These DC electrical transport properties indicate the

\*Contact author: [vita.ilakovac-casses@sorbonne-universite.fr](mailto:vita.ilakovac-casses@sorbonne-universite.fr)

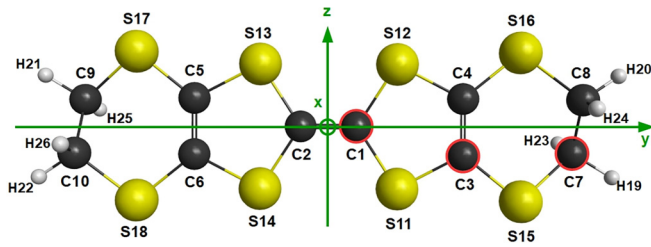


FIG. 1. Geometry of an isolated BEDT-TTF (ET) molecule. It is optimized in the  $D_2$  point group, where it has three twofold axes,  $x$ ,  $y$ ,  $z$ , indicated by green arrows, and three nonequivalent carbon sites, C1 (central), C3 (side), and C7 (terminal ethylene), indicated by red circles.

inherent heterogeneity present in the system such that the system should be more properly described as a Mott-Anderson insulator [10]. Similarly, the relaxorlike dielectric response in the insulating state below 60 K, controversially discussed for years [9,11], most likely results from inhomogeneities since no clear experimental evidence of electric dipoles was found [12]. Namely, common refinement of the structure of  $\kappa$ -Cu is usually performed in the monoclinic and centrosymmetric  $P2_1/c$  space group [2,13–19], thus excluding the presence of electric dipoles at all temperatures. However, recent structural results by Foury *et al.* [20], collected between 300 and 3 K, evidence a symmetry breaking, revealing that the structure is triclinic. The space group is lowered to  $P\bar{1}$  or even  $P1$ , meaning that there are at least two nonequivalent dimers in the unit cell. However, analysis of structural refinements performed at 300 and 100 K with the help of density functional theory calculations finds only a tiny *interdimer* charge imbalance of 0.06e, which is close to the resolution limit. Unfortunately, due to technical difficulties, the low-temperature structure (below 100 K) could not be refined. Importantly, a recent Raman study by Liebman *et al.* [21] shows that no phase transition occurs down to 6 K, while a negligibly small, fluctuating, charge imbalance of 0.05e (assumed to be *intradimer*) develops below 60 K. We point out that the assumption of *intradimer* charge imbalance could

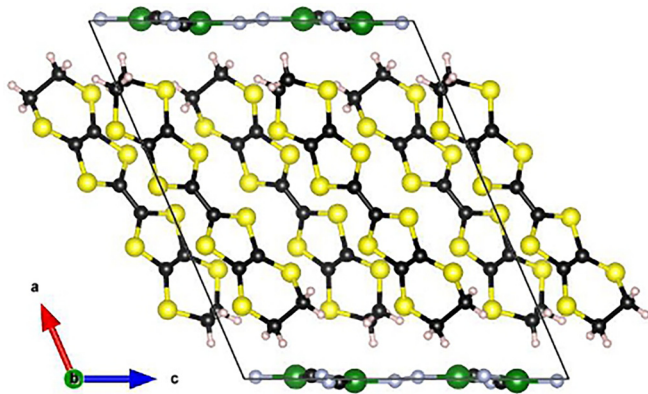


FIG. 2. Side view of the  $\kappa$ -(BEDT-TTF) $_2$ Cu $_2$ (CN) $_3$  ( $\kappa$ -Cu) structure, showing layers of BEDT-TTF (ET) molecules separated by anion planes. Carbons are black, sulfurs are yellow, nitrogens are gray, coppers are green, and hydrogens are rose color.

only be possible if the space group is  $P1$ . But that possibility remains unproven since the x-ray measurements are not able to discriminate between the  $P1$  and  $P\bar{1}$  space groups. Last but not least, *interdimer* charge imbalance, in line with the results in Foury *et al.* [20], was recently suggested to also be relevant in another  $\kappa$ -(BEDT-TTF) $_2X$  system based on the Raman spectra calculations and analysis [22].

The  $\kappa$ -Cu molecular dimers, each hosting  $S = 1/2$  spin, form a relatively highly frustrated triangular lattice with large exchange coupling of  $J = 250$  K, but without any magnetic ordering [6]. Initially, the suppression of the magnetic state was primarily attributed to frustration. Indeed, if  $\kappa$ -Cu had Ising spins with antiferromagnetic coupling on a perfectly equilateral two-dimensional (2D) triangular lattice, the spins would be entirely frustrated without the possibility of any order in the ground state. But  $\kappa$ -Cu is a Heisenberg antiferromagnet, where spins can rotate in the  $(b,c)$  plane. Such a triangular lattice, when perfectly equilateral, can host a spin  $120^\circ$  order, which is not observed [23]. In addition, in  $\kappa$ -Cu, there is a slight anisotropy of transfer integrals [13,24], indicating that the triangular lattice is not perfectly equilateral. Thus growing evidence indicates that the degree of frustration in  $\kappa$ -Cu might not be enough to host a QSL [1,25], and that disorder or randomness may play an equally important role [8,26]. Recently, however, an opening of a spin gap was evidenced, pointing to a nonmagnetic ground state, described as a singlet valence-bond state [27–29]. While this finding rules out a gapless scenario with mobile spinons, it still leaves open the possibility of a gapped QSL phase. Most importantly, it highlights that the nature of the ground state is strongly affected by disorder, as also suggested from the conductivity and the dielectric properties' behavior at higher temperatures [9,10].

Already the coupling of organic molecules to the anion layers via the ethylene groups imposes disorder. Indeed, in all ET compounds, side ethylene groups, pointing to the anion layer, can take different conformations relative to the plane defined by the rest of the molecule. The disorder of ethylene groups is likely dynamical at high temperature, while progressively quenching at low temperature. Anion planes offer an additional type of disorder, as the bridging cyanide groups can take two orientations relative to the Cu atoms. Both subsystems thus contribute to the inherent disorder of the compound. This can be viewed as large-scale charge inhomogeneities onto the BEDT-TTF layer, as has been demonstrated by combined numerical and spectroscopic studies which clearly uncover the importance of the Cu $_2$ (CN) $_3$  anion network coupled to the ET molecules [30].

Finally, the question arises of how the lattice dynamics couples to charge and spin degrees of freedom; in other words, to what extent the electron-phonon coupling (EPC) is relevant in  $\kappa$ -Cu. In our previous work [31], we tuned the incident light energy at the  $K$ -edge of nitrogen sites, which enabled us to study excited phonon modes in the anionic layers. Combining measured data with numerical calculations permitted us to estimate the site-dependent EPC of these modes to contribute at least 20% to the total ET molecular-layer EPC. The latter was previously extracted from infrared and Raman data obtained for  $\beta$ -(ET) $_2$ I $_3$  by Girlando *et al.* [32] using the quasiharmonic lattice dynamics.

In order to shed more light and deepen the understanding of the excitation properties in  $\kappa$ -Cu, we have conducted C  $K$ -edge near-edge x-ray absorption fine structure (NEXAFS) and resonant inelastic x-ray scattering (RIXS) measurements at 300 K and at 15 K. A comparison of these data with our calculations of the NEXAFS spectra performed on an isolated BEDT-TTF molecule permits us to identify different carbon sites contributing to the pre-edge features of the NEXAFS spectrum. The full  $\kappa$ -Cu crystal calculation provides evidence that the environment of each of these carbon sites is already strongly disturbed by the static disorder in the structure. Moreover, RIXS measurements do not show a clear set of vibrational harmonics, but point toward a complex multimode vibrational excitation spectra, indicating additional strong dynamical disorder in the system. In contrast to previous N  $K$ -edge results, no monomode excitation with resolved harmonics was detected, thus disabling us from estimating the molecular plane mode's contribution to the total EPC of the  $\kappa$ -Cu.

## II. EXPERIMENTAL AND CALCULATION DETAILS

### A. Experimental details

High-quality single-crystal samples of  $\kappa$ -Cu were grown using the electrocrystallization method [2,33]. C  $K$ -edge NEXAFS data were acquired at the TEMPO beamline [34,35] of the synchrotron SOLEIL. The room-temperature signal was collected in the total electron yield (TEY) mode with the beamline resolution set to 110 meV and with the linear horizontal light polarization. RIXS measurements were performed at the SEXTANTS beamline [36] of the synchrotron SOLEIL by means of the AERHA spectrometer [37] with an overall energy resolution of 120 meV. The scattering angle was fixed to  $85^\circ$  and the incident light polarization was linear horizontal. RIXS measurements were performed at 300 and 15 K. In both measurements, data were recorded in grazing incidence geometry, with the incoming photon polarization ( $\varepsilon$ ) almost perpendicular to the anion layer  $\angle(\varepsilon, a^*) = 20^\circ$ , where  $a^*$  stays for the reciprocal lattice vector perpendicular to the  $(b,c)$  plane. The orientation of the  $b$  and  $c$  axes with respect to the scattering plane was not determined.

### B. Calculation details

Calculations performed on the isolated BEDT-TTF molecule were done using the density functional theory (DFT) with Becke three-parameter hybrid exchange [38] and the Lee-Yang-Parr gradient-corrected correlation functional [39] (B3LYP) implemented in the GAMESS(US) program [40]. The 6-31G\* basis set was used [41]. The geometry optimization was performed for the ground state with different constraints on the symmetry of the molecule. Transition probabilities (oscillator strengths) and the relative excited energies were calculated by the configuration-interaction method (CI) in the Hartree-Fock approximation. The transition energies to the first (excited-state) unoccupied orbitals are further set on their  $\Delta$  Kohn-Sham ( $\Delta$ KS) value, computed for a triplet final state. The relativistic correction of 0.2 eV for carbon has been included [42].

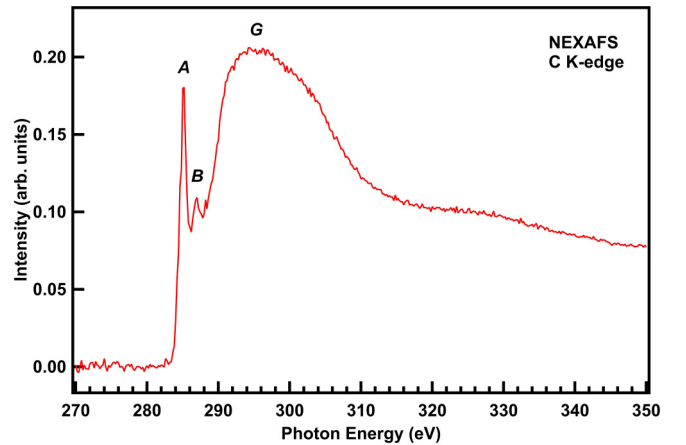


FIG. 3. NEXAFS spectrum of  $\kappa$ -Cu measured at the C  $K$ -edge at room temperature using horizontal light polarization.

Calculations performed on the full  $\kappa$ -Cu crystal structure were done by the finite difference method near-edge structure (FDMNES) code, which is an all-electron code taking into account the presence of the core hole. [43–45]. These density functional theory calculations were performed using atomic orbitals as a basis set and the Hedin and Von Barth [46] functional.

## III. RESULTS

### A. Experimental spectra

A large energy-scale C  $K$ -edge NEXAFS spectrum, measured at 300 K, is presented in Fig. 3. It shows a pre-edge structure characterized by two sharp features in the photon energy ( $h\nu$ ) range of 284–288 eV, indicated as A and B, respectively: one strong peak at  $h\nu_A = 285.1$  eV and a smaller peak at  $h\nu_B = 286.8$  eV. They are followed by a broad structure above the edge, which extends from 288 to 310 eV. It will be indicated by G.

Figure 4 shows overall room-temperature RIXS spectra measured at the C  $K$ -edge. They are presented in the emitted energy scale, where the position of the narrow and strong elastic peak shifts with the excitation energy. The spectra are characterized by two broad features centered at constant emitted energy of about 277 eV ( $\alpha$ ) and 281 eV ( $\beta$ ), showing fluorescent behavior. The intensity of the structure  $\alpha$  strongly increases at the incident photon energy  $h\nu_A = 285.1$  eV, where the intensity of the elastic peak presents a maximum as well. The elastic peak has a symmetrical line shape far from the resonance, at  $h\nu = 288.1$  eV. But for photon energies close to  $h\nu_A$ , it shows an asymmetric line shape, with a shoulder on its low emitted energy side, and following the elastic peak as the incident photon energy is changed.

In order to unravel excitations contributing to the low emitted energy shoulder of the elastic peak, we measured low-temperature (15 K) RIXS spectra close to the C  $K$ -pre-edge maximum,  $h\nu_A = 285.1$  eV. The spectra are presented in Fig. 5, in the energy loss scale ( $E_L$ ), with the constant elastic peak position at  $E_L = 0$ . They reveal that the structure  $\alpha$  is composed of two features which resonate at  $h\nu_A = 285.1$  eV, and form two sharp peaks, at  $E_L = -6.87$  eV and  $-8.51$  eV.

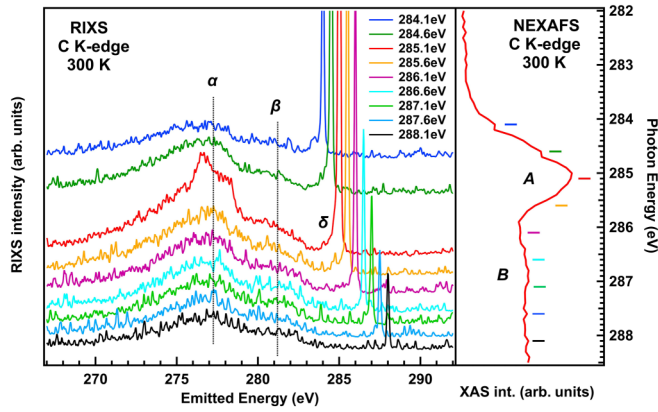


FIG. 4. Room-temperature RIXS (left) and NEXAFS (right) spectra measured on  $\kappa$ -Cu at the C  $K$ -edge and with the linear horizontal light polarization. Incident photon energies of the RIXS spectra are indicated by lines of the corresponding color in the NEXAFS spectrum. RIXS spectra are shifted at the intensity scale for clarity.

They are attributed to the interorbital excitations which are resonantly reinforced at the NEXAFS pre-edge maximum. Close to the elastic peak, for  $E_L$  between  $-1$  and  $0$  eV ( $\delta$ ), there is an intensity increase, resulting in an asymmetric shape of the elastic peak. It points to the presence of unresolved low-energy excitations which are reinforced at the excitation energy corresponding to the carbon pre-edge peak.

### B. NEXAFS pre-edge calculation considering an isolated BEDT-TTF (ET) molecule

A formula unit of  $\kappa$ -Cu has 23 carbon atoms. 20 of them are in two ET molecules and only three are in the anion layer. In order to identify contributions of different carbon sites to the C  $K$ -pre-edge NEXAFS, we first present the calculation performed on an isolated ET molecule. We chose its  $D_2$  point-group geometry, already used for the calculations of charge-sensitive vibrational modes of  $\text{ET}^0$

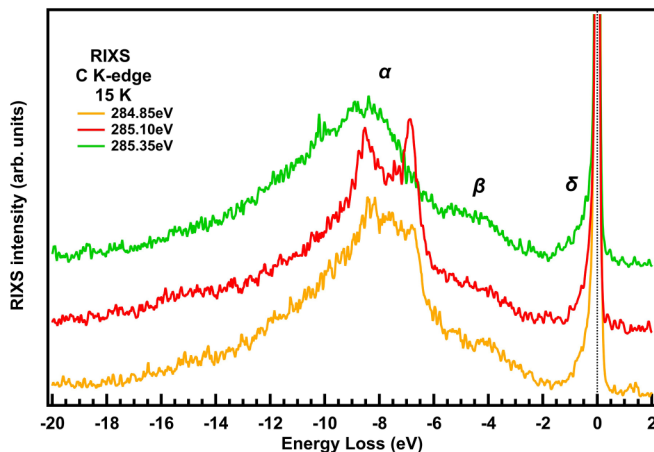


FIG. 5. RIXS spectra on  $\kappa$ -Cu measured across the C  $K$ -pre-edge maximum, at the temperature of 15 K and with the linear horizontal polarization.

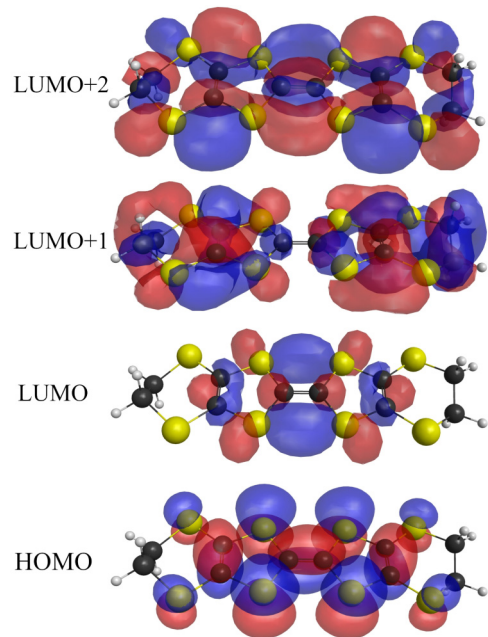


FIG. 6. HOMO and three lowest unoccupied orbitals of the ground-state ET molecule in the  $D_2$  point group. Red/blue colors indicate the positive/negative sign of the molecular orbital wave function.

neutral,  $\text{ET}^+$  charged molecule, and  $\text{ET}_2^+$  dimer [22,47]. Even if this symmetry does not give the equilibrium geometry of the ET molecule, it is quite close to the geometry of the more probable conformation of the ET molecule in the  $\kappa$ -(BEDT-TTF) $_2$ Cu $_2$ (CN) $_3$  crystal. Different geometries of the ET molecule and its conformations in the  $\kappa$ -(BEDT-TTF) $_2$ Cu $_2$ (CN) $_3$  structure, as well as the validation of the choice of the geometry used for the NEXAFS calculation, are described in detail in the Supplemental Material [48] (including Refs. [49,50]).

The ET molecule has 98 occupied orbitals in its ground state (GS), i.e., the initial state of the absorption process. In the  $D_2$  point group, 26 of them are of  $A$  symmetry, 23  $B_1$ , 25  $B_2$ , and 24  $B_3$ . The last and highest occupied molecular orbital (HOMO) is the 24th  $B_3$  and has  $\pi_\perp$  character; see Fig. 6. It is delocalized on the whole molecule, even if its weight on ethylene groups is quite low. The first and lowest unoccupied orbital (LUMO) has  $\sigma$  character (27  $A$ ). Its weight is mostly localized in the central part of the molecule. LUMO+1 is the 24th  $B_1$ , has a mixed  $\pi_\parallel$  and  $\sigma$  character, and is delocalized on the moieties of the molecule, but not in the central part. LUMO+2 has  $\pi_\parallel$  character (26  $B_2$ ) and is delocalized on the whole molecule.

Transition probabilities (oscillator strengths) and relative energies for the C  $1s$  excitation below the ionization potential (IP = 291.680 eV) are given in Table I. Note that the order of the orbitals in the excited state is not the same as in the ground state. The process of accommodation of a core electron into a particular valence state can act differently on the stabilization of different orbitals, i.e., some orbital states can be stabilized more than others. This is particularly the case of the first C1-site excited state, which is LUMO+1.

TABLE I. Calculated ET molecule C  $1s$  excitation energies and probabilities below the ionization potential (IP).

Carbon site	Final state orb. sym.	Order rel. to GS	Transition energy (eV)	Transition probability osc. strength
C1	24 $B_1$	+1	287.392	0.036392
	27 $A$	LUMO	287.642	0.006004
	26 $B_2$	+2	288.572	0.044174
	28 $A$	+3	289.582	0.004758
	25 $B_1$	+5	289.852	0.001060
	25 $B_3$	+6	290.192	0.000017
	27 $B_2$	+4	290.712	0.001327
	29 $A$	+9	291.112	0.005365
	26 $B_1$	+7	291.452	0.003782
C3	27 $A$	LUMO	287.678	0.021023
	24 $B_1$	+1	288.268	0.036319
	25 $B_3$	+6	290.198	0.012427
	26 $B_2$	+2	290.438	0.006185
	28 $B_2$	+8	290.648	0.000592
	28 $A$	+3	291.048	0.017893
C7	27 $A$	LUMO	288.156	0.034763
	27 $B_1$	+12	290.696	0.006963
	26 $B_2$	+2	291.096	0.006641
IP			291.680	

Figure 7 shows the experimental NEXAFS C  $K$ -pre-edge of  $\kappa$ -Cu and compares it to the calculation on an isolated ET molecule.

The intensity bars, corresponding to the different excitations given in Table I, are convoluted by Lorentzian profiles whose width,  $\Gamma = 0.15$  [51], includes the C  $1s$  core-hole lifetime,  $\Gamma_{1s} = 0.11$  eV [52], and the experimental broadening,  $\gamma = 0.11$  eV.

The calculation on an isolated ET molecule quite well describes the two main features in the pre-edge,  $A$  and  $B$ ,

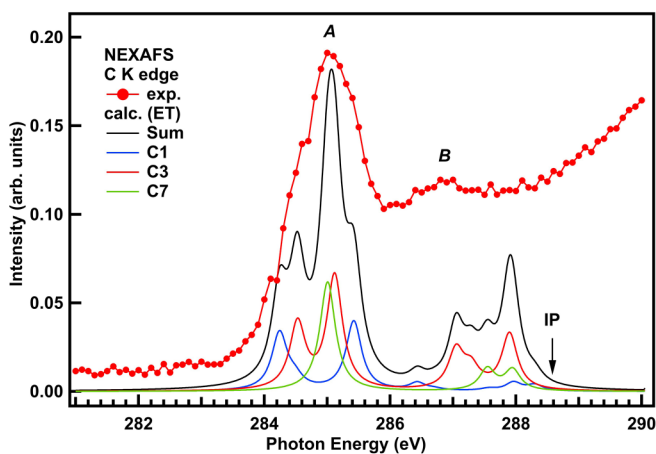


FIG. 7. Experimental C  $K$ -pre-edge NEXAFS spectrum of  $\kappa$ -Cu (red points) compared to the calculations performed on an isolated ET molecule (black line). Contributions from C1, C3, and C7 sites are shown by blue, red, and green lines, respectively. Calculated spectra are shifted for  $-3.1$  eV in order to match the experiment.

including the low- and high-energy shoulder of the main peak. It shows that the three ET nonequivalent carbon atoms contribute to the pre-edge, but in different ways. The pre-edge maximum ( $A$ ) is described mostly by the side-C3 and the ethylene-C7 cross sections, while the central-C1 contributes to its shoulders. The small structure  $B$  has mostly C3 contribution. Note that the intensity of the C3 and C7 features is multiplied by 2, as the number of these sites is twice the number of C1 sites.

We remark that this calculation does not include states above the ionization potential (IP) as they are considered to be itinerant. The intensity above the edge, defined as IP, is put to zero.

### C. NEXAFS calculation on the full $\kappa$ -Cu structure

In the following, we wish to analyze how the x-ray absorption cross section of the three nonequivalent molecular sites C1, C3, and C7 is modified in the  $\kappa$ -Cu crystal environment. We thus performed the calculation on the full  $\kappa$ -Cu structure, where ET molecules form charged (+1) dimers. In addition, the structure of  $\kappa$ -Cu is known to exhibit disorder in the anion plane as well as in the ET molecular layer [2,14–17,20]. The output of structural refinements of this system gives atomic positions where some sites have partial occupation.

The data from the  $\kappa$ -Cu structural refinement by Foury *et al.* [20] have been chosen for the full crystal calculation. This refinement was performed in the triclinic space group  $P\bar{1}$ , contrary to previous works [2,13–19], which were performed in the monoclinic and centrosymmetric  $P2_1/c$  space group.

X-ray scattering factors of C and N being almost identical, preferential orientation of CN groups bridging the -Cu-CN-Cu- polymeric chains in the anionic layer could not be determined by any structural refinement. Thus, bridging C(N) atoms were considered as having 50:50 C/N partial occupation. For the disorder in the molecular layer, in the refinement which we used, the conformation of ET molecules has been determined to be staggered (S: t,t) with 72% probability and eclipsed (E: t, $\bar{t}$ ) with 28% probability, which is the proportion close to the values previously determined previously [13,19].

For the sake of electronic structure calculations, these partial occupations had to be eliminated. In a double  $\kappa$ -Cu unit cell of 240 atoms, an alternation of orientations of bridging CN groups was applied in the  $b$  direction. Further, the more probable S(t,t) conformation has been chosen for all the ET molecules. The symmetry was thus lowered to  $P1$  and the unit cell contained four formula units and thus four dimers.

FDMNES calculations on this  $P1$   $\kappa$ -Cu structure show that all 92 carbon sites are nonequivalent by symmetry. For the sake of clearness, the carbon sites are sorted into five groups and presented by different colors in the figures. For the ET molecule carbons, the same colors as in the calculation on the isolated ET molecule (see Fig. 7) are used: blue for 16 central-C1, red for 32 side-C3, and green for 32 terminal ethylene-C7 carbons. The two groups of carbons in the anion plane, eight in the chains and four bridging the chains, are indicated by gray and black lines, respectively.

The experimental NEXAFS spectrum is compared to the FDMNES calculation in Fig. 8. The first structure of the NEXAFS pre-edge, at 285.1 eV, denoted by  $A$ , is almost perfectly

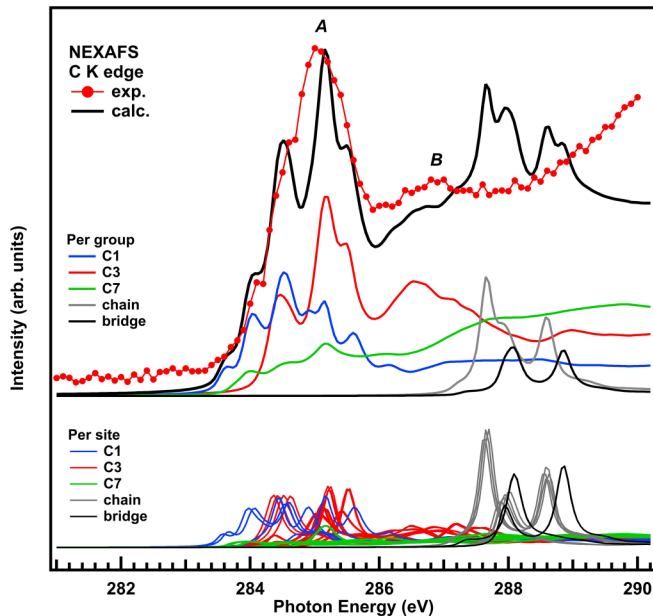


FIG. 8. Experimental C *K*-pre-edge NEXAFS spectrum of  $\kappa$ -Cu compared to the calculation using the structural refinement by Foury *et al.* [20]. The sum of the contributions from the groups of carbon atoms is indicated blue, red, green, gray, and black lines. The spectral weight of each nonequivalent carbon site, presented in the same scale, but multiplied by 4 for clearness, is shown at the bottom of the figure.

reproduced by the calculation. It has a strong contribution from the three ET carbons, in particular the side-C3 site, and the central-C1 site, which dominates at low energy. The contribution from the ethylene-C7 site is weakened, compared to the isolated ET calculation, and does not present strong and sharp features.

The second structure, at 287 eV, denoted by *B*, is well described in the full crystal  $\kappa$ -Cu calculation. Its spectral weight is due to the contribution from the side-C3 site.

At higher energy, the calculation on the  $\kappa$ -Cu structure predicts a strong feature attributed to the anion plane (bridge and chain) carbons, which does not match well with the experimental data. Its energy is too high to be related to the second pre-edge structure at 287 eV. The large feature centered at 297 eV, indicated by *G* (see Fig. 9) is not very well reproduced by the calculation. At position *G*, the calculation predicts an increased spectral weight of the three ET carbons, in particular of the central-C1 and the side-C3 sites, but its intensity is too low.

Note that the high-energy part of the spectra is not included in the calculation on the isolated ET molecule.

## IV. DISCUSSION

### A. Discussion: NEXAFS spectrum

As pointed out in Sec. III B for the calculation on the isolated ET molecule, its three nonequivalent carbon atoms contribute to the strong peak in the C *K*-pre-edge. The central-C1 and the side-C3 carbon contribute to the low-energy shoulder of the feature *A* (see Fig. 7), while the intensity maximum is due to side-C3 and ethylene-C7 carbons. The

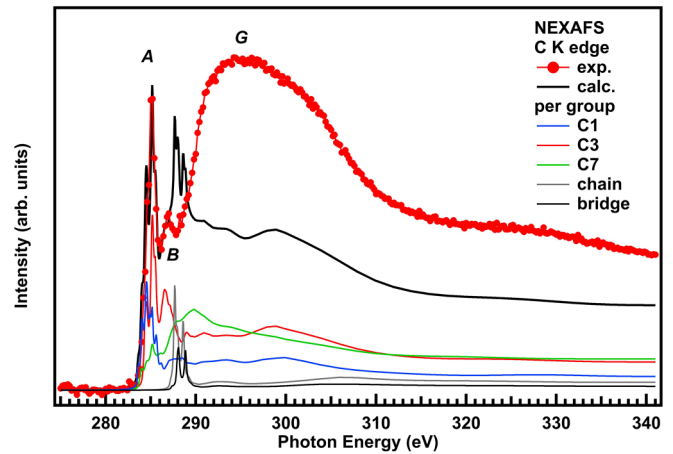


FIG. 9. Experimental C *K*-edge NEXAFS spectrum of  $\kappa$ -Cu (red points) compared to the calculation (black line) using the structural refinement by Foury *et al.* [20]. Other spectra (colored lines) are calculated contributions from different specific carbons (see text for identification).

small structure at higher energy (denoted by *B* in Fig. 7) has mostly C3 and C7 contributions. The total intensity is described by only three spectra, one for each nonequivalent site, sites C3 and C7 contributing twice as their number in the molecule is twice the number of C1 sites.

In the *P1* space-group full-crystal calculation, each site has its own spectrum, as all the C sites are nonequivalent by symmetry. This gives a bunch of spectra for each group of atoms (C1, C3, C7, chain, bridge); see lower part of Fig. 8 (“per site”). One can still recognize that the pre-edge has strong contributions from the ET carbons. The calculation on an isolated ET molecule permits one to identify the sites which contribute to the pre-edge. It cannot, however, predict the complexity of these spectra as it does not take into account the complex environment of each carbon site inside the crystal.

In order to discuss the details of the calculated NEXAFS spectra on a clearer basis, we first present the view along the *a* axis [Fig. 10(a)] and *b* axis [Fig. 10(b)] of the *P1* space-group structure, and two nonequivalent dimers D1 [Fig. 10(c)] and D2 [Fig. 10(d)]. Carbon atoms are labeled solely by their numbers, i.e., 11–20 for the dimer D1, 21–30 for the dimer D2, while other atoms, i.e., sulfur and hydrogen, are not labeled. Note that the positions of carbons 20 and 30 are split in the structure, as they can be in the ethylene group which has, besides the actual staggered, the eclipsed conformation. Particular carbon sites, which will be discussed in the following, are indicated by cyan (D1) and orange (D2) colors.

The effect of the environment on the site-projected NEXAFS spectra is shown in Fig. 11, where the calculated spectra of the isolated molecule are compared to these in the full-crystal structure, for sites (group of sites) C7 [Fig. 11(a)], C3 [Fig. 11(b)], and C1 [Fig. 11(c)]. As explained in Sec. III C, the inversion symmetry in the  $P\bar{1}$  space group had to be broken for the sake of electronic structure calculations. However, in the bunch of spectra of different sites in the crystal, the carbon sites which were related by the inversion symmetry in the  $P\bar{1}$  have almost identical spectra. For the sake of clearness, in

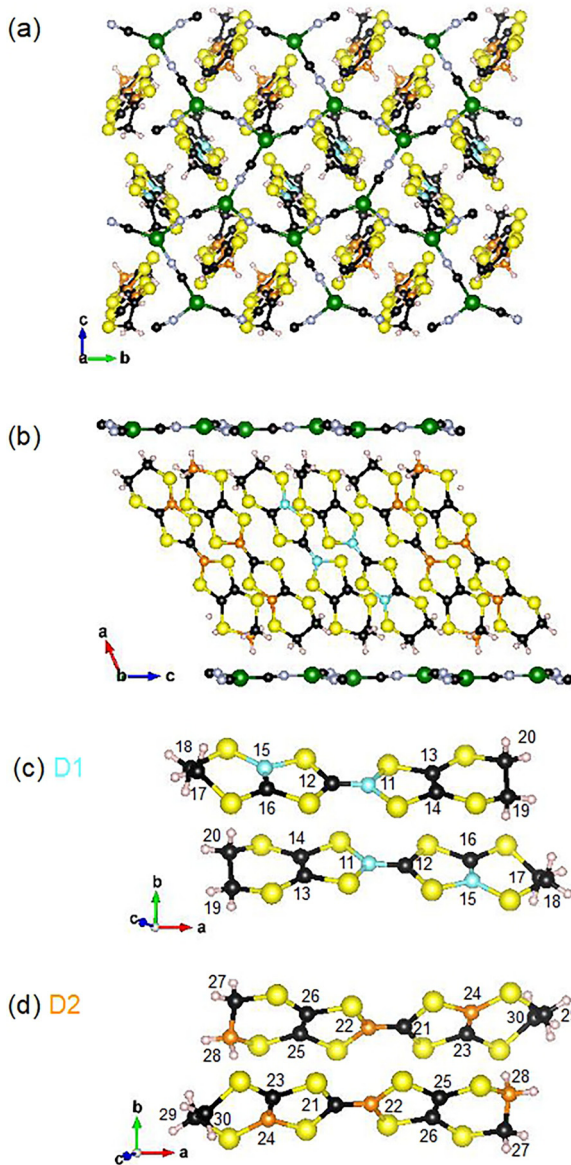


FIG. 10. Molecular layer and an anion layer of a  $P1$  space-group structure, view along its (a)  $a$  axis and its (b)  $b$  axis, and its two (strongly) nonequivalent dimers (c) D1 and (d) D2. Particular carbon sites, with the highest intensity maximum in the NEXAFS calculation of Fig. 11, are indicated by cyan and orange colors, for D1 and D2, respectively.

Fig. 11, only one of four of them is shown. Moreover, the color code of the carbon sites, which will be discussed in the following, is different in the two dimers (D1, D2), i.e., cyan for D1 and orange for D2.

Note that in Figs. 11(a)–11(c), different sites of each group have very different spectra. It is interesting to note that this diversity is not present only in the ethylene-C7 group, but as well in the side-C3 and central-C1 groups. We remark that the terminal ethylene-C7 group is at the frontier of the two subsystems (ET layer and anion plane). The ethylene-C7 group is also at the source of the disorder in the system, as the conformation of ET molecules can be staggered or eclipsed. In addition, some of the ethylene sites are close to the anion plane C or N bridge, which are orientationally

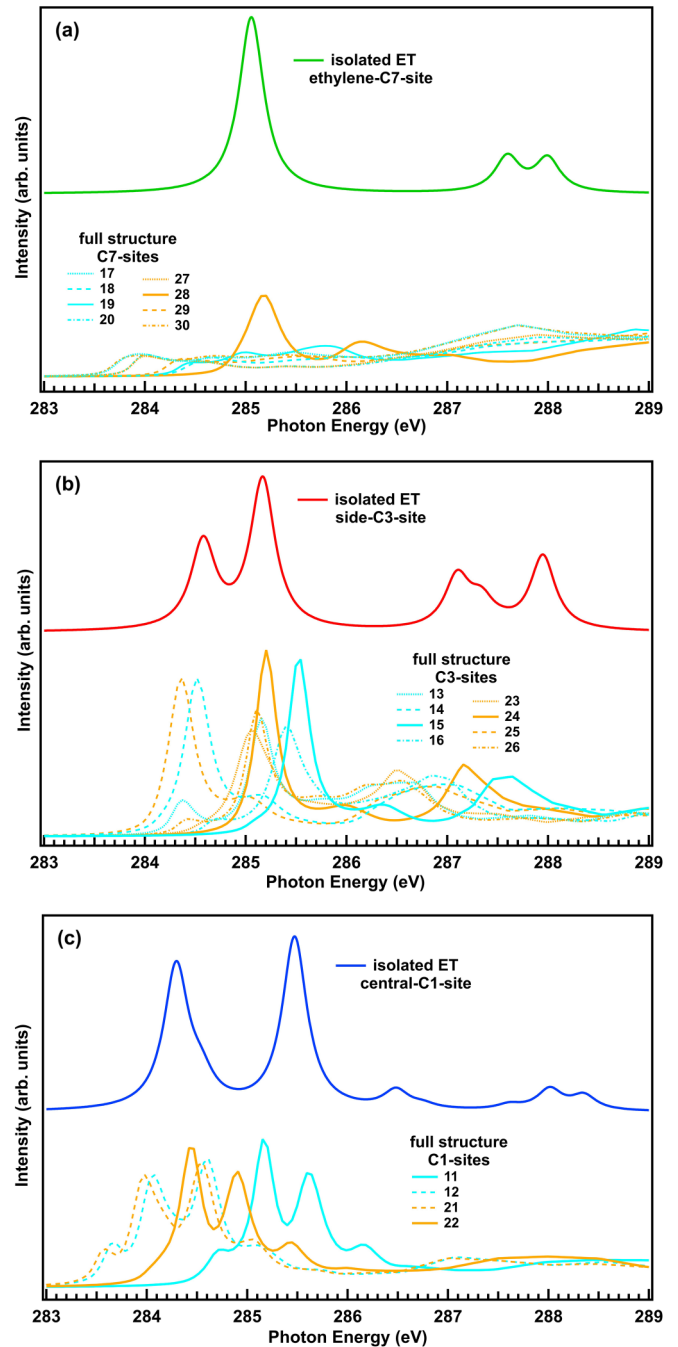


FIG. 11. Site-dependent calculation on an isolated ET and in the full crystal: (a) for the ethylene-C7 site, (b) for the side-C3 site, and (c) for the central-C1 site. The color of the spectra of particular carbon sites corresponds to those in Fig. 10.

disordered. Thus, for this group of sites, one would expect that the disordered environment results in a bunch of completely different spectra, which is effectively the case. But for the sites C3 and C1, which are inside the molecule, a set of more similar spectra is expected.

In Fig. 11(a), the spectrum of one of the ethylene-C7 sites, labeled as 28 in Fig. 10, has a strong maximum and completely differs from the rest of the ethylene-C7 group. Note that its position, indicated by orange color, is in dimer D2. Figure 11(b) shows that the side-C3 spectra of D1 are at higher

photon energy compared to the D2 spectra. This is particularly clear for the sites 15 (D1) and 24 (D2). The shift between the D1 and the D2 spectra is even increased in the case of the central-C1 sites 11 (D1) and 22 (D2).

A very simple explanation of the relative shift of the spectra is due to the so-called chemical shift, which can be related to the charge of a particular site: the more the charge of a site is negative, the more its spectrum is shifted to a higher photon energy. In this sense, we can identify two ranges of nonequivalent dimers in terms of charge distribution [see Fig 10(a)], even if their global charge is not significantly different, which is in line with the work by Foury [20] and Girlando [22], who support interdimer charge imbalance. In addition, it is possible that ET molecules in each dimer have permanent dipoles, which are oriented in opposite directions. Let us remind the reader that we calculated NEXAFS spectra for only one configuration of CN bridge orientation and only choosing staggered twisting of all the ET molecules. In the real structure, there is an orientational disorder of bridging CN groups as well as the possibility of the eclipsed conformation of the ET molecules, meaning that the distribution of charge on a particular molecule is altered as a consequence, inducing an additional disorder.

At 288.4 eV, the calculation on the  $\kappa$ -Cu structure predicts a sharp doublet attributed to the anion plane (bridge and chain) carbons,; see Fig. 8. Its intensity, however, is too high and does not match well with the experimental data. Above 290 eV, there is a broad feature *G* in the experimental spectra, with a maximum at about 295 eV (see Fig. 9). The calculated spectral weight of the three ET carbons, in particular of the C1-central and the C3-side sites, has an increase at 3 eV higher energy compared to the maximum of the feature *G*. But this intensity increase is not sufficient to describe the whole feature *G*.

The discrepancies between the experiment and the calculation above the edge could have either an experimental or theoretical origin. First, on the black surface of the crystals, we observed micrograins of white color (see Supplemental Material, Ref. [48]). These could be due to some residuals of the solvent used to prepare the crystals. They should contain amounts of noncrystallized carbon in some form. Such amorphous amounts of carbon show up a broad feature above the C *K*-edge. Additionally, we detected small radiation damage effects in resonant RIXS spectra, measured at the incident energy indicated by *A* in the NEXAFS spectra. The study of this beam damage showed that it does not change the general spectral shape, but has only a minor effect on relative intensities. We are therefore confident that our results remain valid and reflect the intrinsic properties of the studied samples. Second, for each nonequivalent carbon, the FDMNES calculation is performed on a cluster of a 7 Å radius, which is centered on this particular carbon site. When the cluster is centered on anion layer carbons, it does not include all nonequivalent carbon sites. Ethylene sites are all included, but half of the side carbons and all central carbons are out of the cluster range.

### B. Discussion: RIXS spectra

As shown in Figs. 4 and 5, the elastic peak presents an asymmetric line shape resulting from a resonantly enhanced

shoulder on the energy-loss side extending up to about 1 eV. This feature is a signature of low-energy excitations that are visible in the RIXS spectra at the excitation energy close to the maximum of the pre-edge,  $h\nu_A = 285.1$  eV, indicated in the NEXAFS spectrum as the structure *A*. NEXAFS calculations show that this photon energy corresponds mostly to the excitation of the C3-side sites of the ET molecule in the  $\kappa$ -Cu structure. As the sample is insulating, we do not expect any contribution arising from delocalized states at this photon energy. The low-energy excitations close to the elastic peak are most probably due to phonon excitation.

Recent publications show that resonant x-ray inelastic scattering (RIXS) permits one to directly measure the electron-phonon coupling (EPC) [31,53–56]. It can be deduced from the envelope of the vibrational progression close to the elastic peak [53]. It has been applied to estimate the EPC of a localized (Einstein) mode in titanates [55,56] and in cuprates [57]. RIXS measurements at the N *K*-edge were successfully used to estimate the contribution of the anion plane modes to the  $\kappa$ -Cu EPC [31].

But contrary to the N *K*-edge excitation [31] of the same system, there are no vibrational harmonics of a particular mode that can be clearly resolved at the C *K*-edge. In the case of the N *K*-edge, tuning the photon energy at the nitrogen site of the ordered (chain) cyano group switched five distinct harmonics of the anion plane CN stretching mode. Conversely, tuning the excitation energy on the one corresponding to the disordered (bridging) sites revealed a multimode excitation. This permitted us to determine the EPC of selected CN modes and to relate it to the environment and the dynamics of nonequivalent nitrogen sites.

One should note that contrary to NEXAFS, whose broadening depends on the lifetime of the C *K*-edge excited state ( $\Gamma_{1s} = 0.1$  eV [52]), RIXS natural broadening is much smaller as it depends on the lifetime of a valence-excited state (the final state of the RIXS process) which is negligible. RIXS resolution is thus limited by the experimental resolution of 120 meV. We could thus expect to observe vibrational modes with an energy higher than 120 meV, such as CN stretching at 250 meV ( $2100\text{ cm}^{-1}$ ) and, in particular, C = C stretching at about 180 meV ( $1430\text{ cm}^{-1}$ ), as the photon energies close to  $h\nu_A = 285.1$  eV correspond to the C3-site excitation. As this is not the case, we conclude that in  $\kappa$ -Cu, at the C *K*-edge, stretching modes are not solely excited. There is a strong multimode vibrational excitation likely related to all the nonequivalent carbon sites in the ET molecule. The RIXS calculation including multimode vibrational excitation is a highly complex task, which falls outside the scope of the present work. However, a tentative calculation of the quasielastic part of the RIXS spectra is presented in the Supplemental Material [48].

### C. Discussion: Disorder

Kawamoto *et al.* observed a remarkable broadening of the nuclear magnetic resonance (NMR) line, indicating the development of inhomogeneities in the charge density upon cooling [58]. Subsequent NMR confirmed this finding and showed that the line broadening becomes strongly enhanced and anomalous at low temperatures ( $T < T^* \approx 6$  K), indi-

cating spatially nonuniform magnetizations induced in the frustrated system under magnetic fields [59]. Importantly, in the former measurements, only a single central carbon of ET molecule was  $^{13}\text{C}$  enriched, while in the latter,  $^{13}\text{C}$  was enriched for the doubly bonded carbon sites at the center of ET. In that sense, NEXAFS and RIXS measurements present an advantage since they allow one to probe the local environment of all carbons (two central, four side, and four terminal) of the ET molecule, as well as of carbons in the anionic layers. In this way, our results shed more light on the origin of disorder observed experimentally to play a crucial role in the physical behavior at high as well as low temperatures in  $\kappa$ -Cu. Disorder is also invoked in theoretical models to help promote the formation of the ground state in  $\kappa$ -Cu. Its important role in the formation of the QSL state has been previously proposed by Watanabe *et al.* [26], whereas more recent theoretical consideration by Riedl *et al.* [28] describes the low-temperature state of  $\kappa$ -Cu as a disorder-induced valence-bond state. Thus, in both models, disorder together with frustration promote the formation of the ground state. Remarkably, the complex interplay between frustration and disorder is observed in a number of novel quantum spin materials; however, a pending task remains to separate the frustration effects from those of disorder [60].

We suggest that the observed effects in  $^{13}\text{C}$  NMR and in our RIXS and NEXAFS measurements, indicating the presence of inhomogeneities, can be accounted for by defects generated in interfaces between frustration-limited domains. The creation of these domains might be triggered by symmetry breaking evidenced by the structural refinements of Foury *et al.* [20]. The latter findings support the existence of low-symmetry domains that are consistent with the overall higher symmetry of the average space group. This is further corroborated by DFT calculations, which help to explain the relaxor-type dielectric response and variable-range hopping transport observed in the insulating state [30]. However, an open question remains regarding whether there is an additional structural modification at 6 K that enhances symmetry breaking and potentially leads to the formation of a nonmagnetic valence-bond state. Notably, a significant change in phonon damping was observed

at 6 K for the breathing mode of BEDT-TTF dimers at  $38\text{ cm}^{-1}$  [30,61].

## V. CONCLUSION

Here we present C  $K$ -edge NEXAFS and RIXS experimental spectra measured on the  $\kappa$ -(BEDT-TTF) $_2$ Cu $_2$ (CN) $_3$  system. NEXAFS spectra are compared to the DFT calculations in order to identify the components of the pre-edge structure. The maximum of the pre-edge is attributed to the carbon atoms in the BEDT-TTF molecular layer, which are all nonequivalent in the  $\kappa$ -(BEDT-TTF) $_2$ Cu $_2$ (CN) $_3$  crystal. The anion plane carbons in the CN groups do not contribute to the NEXAFS maximum, but only to the high-energy small feature of the pre-edge. The elastic peak of the RIXS spectra having an asymmetrical form points to the presence of unresolved multiphonon excitations. Our findings evidence the presence of both static and dynamic disorder in both molecular and anionic layers in  $\kappa$ -(BEDT-TTF) $_2$ Cu $_2$ (CN) $_3$ , and suggest its crucial importance for correlated electronic states, including quantum spin liquid. As previously stated [8], this work once more emphasizes that the full description of the electronic properties of molecular conductors necessitates a complete characterization of the structural coupling and induced disorder between donor and anion layers via the H-bond network. Theoretical models thus need to incorporate the role of disorder at the microscopic level to account for  $\kappa$ -(BEDT-TTF) $_2$ Cu $_2$ (CN) $_3$  physical properties, whereas a precise refinement of the structure at low temperatures remains one of the important experimental tasks which calls for devoted endeavors in future.

## ACKNOWLEDGMENTS

The authors acknowledge the use of the Ceres high performance computer cluster to carry out the FDMNES calculations and the MORPHEUS platform for crystals characterization, both at the Laboratoire de Physique des Solides, Université Paris-Saclay. S.T. thanks Andrej Pustogow for stimulating discussions. This work has been supported by the Labex Palm (Grant No. ANR-10-LABX-0039-PALM).

- 
- [1] M. Dressel and S. Tomić, Molecular quantum materials: Electronic phases and charge dynamics in two-dimensional organic solids, *Adv. Phys.* **69**, 1 (2020).
- [2] U. Geiser Jr., H. H. Wang, K. D. Carlson, J. M. Williams, H. A. Charlier, J. E. Heindl, G. A. Yaconi, B. J. Love, M. W. Lathrop, J. E. Schirber, D. L. Overmyer, J. Ren, and M.-H. Whangbo, Superconductivity at 2.8 K and 1.5 kbar in  $\kappa$ -(BEDT-TTF) $_2$ Cu $_2$ (CN) $_3$ : The first organic superconductor containing a polymeric copper cyanide anion, *Inorg. Chem.* **30**, 2586 (1991).
- [3] Y. Kurosaki, Y. Shimizu, K. Miyagawa, K. Kanoda, and G. Saito, Mott transition from a spin liquid to a Fermi liquid in the spin-frustrated organic conductor  $\kappa$ -(ET) $_2$ Cu $_2$ CN $_3$ , *Phys. Rev. Lett.* **95**, 177001 (2005).
- [4] B. J. Powell, R. H. McKenzie, Quantum frustration in organic Mott insulators: From spin liquids to unconventional superconductors, *Rep. Prog. Phys.* **74**, 056501 (2011).
- [5] K. Kanoda and R. Kato, Mott physics in organic conductors with triangular lattices, *Annu. Rev. Condens. Matter Phys.* **2**, 167 (2011).
- [6] Y. Shimizu, K. Miyagawa, K. Kanoda, M. Maesato, and G. Saito, Spin liquid state in an organic mott insulator with a triangular lattice, *Phys. Rev. Lett.* **91**, 107001 (2003).
- [7] Y. Zhou, K. Kanoda, and T.-K. Ng, Quantum spin liquid states, *Rev. Mod. Phys.* **89**, 025003 (2017).
- [8] J.-P. Pouget, P. Alemany, and E. Canadell, Donor-anion interactions in quarter-filled low-dimensional organic conductors, *Mater. Horiz.* **5**, 590 (2018).
- [9] M. Pinterić, M. Čulo, O. Milat, M. Basletić, B. Korin-Hamzić, E. Tafra, A. Hamzić, T. Ivek, T. Peterseim, K. Miyagawa, K. Kanoda, J. A. Schlueter, M. Dressel, and S. Tomić, Anisotropic charge dynamics in the quantum spin-liquid candidate  $\kappa$ -(BEDT-TTF) $_2$ Cu $_2$ (CN) $_3$ , *Phys. Rev. B* **90**, 195139 (2014).

- [10] M. Čulo, E. Tafra, B. Mihaljević, M. Basletić, M. Kuveždić, T. Ivek, A. Hamzić, S. Tomić, T. Hiramatsu, Y. Yoshida, G. Saito, J. A. Schlueter, M. Dressel, and B. Korin-Hamzić, Hall effect study of the  $\kappa$ -(ET)<sub>2</sub>X family: Evidence for Mott-Anderson localization, *Phys. Rev. B* **99**, 045114 (2019).
- [11] M. Abdel-Jawad, I. Terasaki, T. Sasaki, N. Yoneyama, N. Kobayashi, Y. Uesu, and C. Hotta, Anomalous dielectric response in the dimer Mott insulator  $\kappa$ -(BEDT-TTF)<sub>2</sub>Cu<sub>2</sub>(CN)<sub>3</sub>, *Phys. Rev. B* **82**, 125119 (2010).
- [12] K. Sedlmeier, S. Elsässer, D. Neubauer, R. Beyer, D. Wu, T. Ivek, S. Tomić, J. A. Schlueter, and M. Dressel, Absence of charge order in the dimerized  $\kappa$ -phase BEDT-TTF salts, *Phys. Rev. B* **86**, 245103 (2012).
- [13] H. O. Jeschke, M. deSouza, R. Valenti, R. S. Manna, M. Lang, and J. A. Schlueter, Temperature dependence of structural and electronic properties of the spin-liquid candidate  $\kappa$ -(BEDT-TTF)<sub>2</sub>Cu<sub>2</sub>(CN)<sub>3</sub>, *Phys. Rev. B* **85**, 035125 (2012).
- [14] X. Bu, A. Frost-Jensen, R. Allendoerfer, P. Coppens, B. Lederle, and M. J. Naughton, Structure and properties of a new  $\kappa$ -phase organic metal:  $\kappa$ -(BEDT-TTF)<sub>2</sub>Cu<sub>2</sub>(CN)<sub>3</sub>, *Solid State Commun.* **79**, 1053 (1991).
- [15] X. Bu, P. Coppens, Crystal structure of di-[bis-(ethylenedithio)-tetrathiafulvalene] dicopper tri-cyanide, (C<sub>10</sub>H<sub>8</sub>S<sub>8</sub>)<sub>2</sub>Cu<sub>2</sub>CN<sub>3</sub>, *Z. Kristallogr. - New Cryst. Struct.* **212**, 103 (1997).
- [16] H. Yamochi, T. Nakamura, T. Komatsu, N. Matsukawa, T. Inoue, and G. Saito, Crystal and electronic structures of the organic superconductors,  $\kappa$ -(BEDT-TTF)<sub>2</sub>Cu(CN)[NCN<sub>2</sub>] and  $\kappa'$ -(BEDT-TTF)<sub>2</sub>Cu<sub>2</sub>CN<sub>3</sub>, *Solid State Commun.* **82**, 101 (1992).
- [17] G. C. Papavassiliou, D. J. Lagouvardos, A. Terzis, A. Hountas, B. Hilti, J. S. Zambounis, C. W. Mayer, J. Pfeiffer, W. Hofherr, and P. Delhaes, Physical properties in the normal state of the molecular superconductor  $\kappa$ -(BEDT-TTF)<sub>2</sub>Cu<sub>2</sub>(CN)<sub>3</sub>, *Synth. Met.* **61**, 267 (1993).
- [18] T. Koretsune and C. Hotta, Evaluating model parameters of the  $\kappa$ - and  $\beta'$ -type Mott insulating organic solids, *Phys. Rev. B* **89**, 045102 (2014).
- [19] T. Hiramatsu, Y. Yoshida, G. Saito, A. Otsuka, H. Yamochi, M. Maesato, Y. Shimizu, H. Ito, and H. Kishida, Quantum spin liquid: Design of a quantum spin liquid next to a superconducting state based on a dimer-type ET Mott insulator, *J. Mater. Chem. C* **3**, 1378 (2015).
- [20] P. Foury-Leylekian, V. Ilakovac-Casses, V. Balédent, P. Fertey, A. Arakcheeva, O. Milat, D. Petermann, G. Guillier, K. Miyagawa, K. Kanoda, P. Alemany, E. Canadell, S. Tomić, and J.-P. Pouget, *Crystals* **8**, 158 (2018).
- [21] J. Liebman, K. Miyagawa, K. Kanoda, and N. Drichko, Novel dipole-lattice coupling in the quantum spin liquid material  $\kappa$ -(BEDT-TTF)<sub>2</sub>Cu<sub>2</sub>(CN)<sub>3</sub>, *Phys. Rev. B* **110**, 165105 (2024).
- [22] A. Girlando, Raman signatures of the strong intra- and inter-molecular charge oscillations in bis(ethylenedithio)-tetrathiafulvalene (BEDT-TTF)  $\kappa$ -phase salts, *Phys. Rev. B* **110**, 035101 (2024).
- [23] B. Bernu, P. Lecheminant, C. Lhuillier, and L. Pierre, Exact spectra, spin susceptibilities, and order parameter of the quantum Heisenberg antiferromagnet on the triangular lattice, *Phys. Rev. B* **50**, 10048 (1994).
- [24] H. C. Kandpal, I. Opahle, Y.-Z. Zhang, H. O. Jeschke, and R. Valenti, Revision of model parameters for  $\kappa$ -type charge transfer salts: An *ab initio* study, *Phys. Rev. Lett.* **103**, 067004 (2009).
- [25] D. A. Huse and V. Elser, Simple variational wave functions for two-dimensional Heisenberg spin-1/2 antiferromagnets, *Phys. Rev. Lett.* **60**, 2531 (1988).
- [26] K. Watanabe, H. Kawamura, H. Nakano, and T. Sakai, Quantum spin-liquid behavior in the spin-1/2 random Heisenberg antiferromagnet on the triangular lattice, *J. Phys. Soc. Jpn.* **83**, 034714 (2014).
- [27] B. Miksch, A. Pustogow, M. Javaheri Rahim, A. A. Bardin, K. Kanoda, J. A. Schlueter, R. Hübner, M. Scheffler, and M. Dressel, Gapped magnetic ground state in quantum spin liquid candidate  $\kappa$ -(BEDT-TTF)<sub>2</sub>Cu<sub>2</sub>(CN)<sub>3</sub>, *Science* **372**, 276 (2021).
- [28] K. Riedl, R. Valentí, and S. M. Winter, Critical spin liquid versus valence-bond glass in a triangular-lattice organic antiferromagnet, *Nat. Commun.* **10**, 2561 (2019).
- [29] A. Pustogow, Thirty-year anniversary of  $\kappa$ -(BEDT-TTF)<sub>2</sub>Cu<sub>2</sub>(CN)<sub>3</sub>: Reconciling the spin gap in a spin-liquid candidate, *Solids* **3**, 93 (2022).
- [30] M. Dressel, P. Lazić, A. Pustogow, E. Zhukova, B. Gorshunov, J. A. Schlueter, O. Milat, B. Gumhalter, and S. Tomić, Lattice vibrations of the charge-transfer salt  $\kappa$ -(BEDT-TTF)<sub>2</sub>Cu<sub>2</sub>(CN)<sub>3</sub>: Comprehensive explanation of the electrodynamic response in a spin-liquid compound, *Phys. Rev. B* **93**, 081201(R) (2016).
- [31] V. Ilakovac, S. Carniato, P. Foury-Leylekian, S. Tomić, J.-P. Pouget, P. Lazić, Y. Joly, K. Miyagawa, K. Kanoda, and A. Nicolaou, Resonant inelastic x-ray scattering probes the electron-phonon coupling in the spin liquid  $\kappa$ -(BEDT-TTF)<sub>2</sub>Cu<sub>2</sub>(CN)<sub>3</sub>, *Phys. Rev. B* **96**, 184303 (2017).
- [32] A. Girlando, M. Masino, and G. Visentini, R. G. Della Valle, A. Brillante, and E. Venuti, Lattice dynamics and electron-phonon coupling in the  $\beta$ -(BEDT-TTF)<sub>2</sub>I<sub>3</sub> organic superconductor, *Phys. Rev. B* **62**, 14476 (2000).
- [33] T. Komatsu, N. Matsukawa, T. Inoue, and G. Saito, Realization of superconductivity at ambient pressure by band-filling control in  $\kappa$ -(BEDT-TTF)<sub>2</sub>Cu<sub>2</sub>(CN)<sub>3</sub>, *J. Phys. Soc. Jpn.* **65**, 1340 (1996).
- [34] F. Polack, M. Silly, C. Chauvet, B. Lagarde, N. Bergeard, M. Izquierdo, O. Chubar, D. Krizmancic, M. Ribbens, J.-P. Duval, C. Basset, S. Kubsky, and F. Sirotti, TEMPO: a new insertion device beamline at SOLEIL for time resolved photoelectron spectroscopy experiments on solids and interfaces, *AIP Conf. Proc.* **1234**, 185 (2010).
- [35] N. Bergeard, M. G. Silly, D. Krizmancic, C. Chauvet, M. Guzzo, J. P. Ricaud, M. Izquierdo, L. Stebel, P. Pittana, and R. Sergo, Time-resolved photoelectron spectroscopy using synchrotron radiation time structure, *J. Synchrotron Radiat.* **18**, 245 (2011).
- [36] M. Sacchi, N. Jaouen, H. Popescu, R. Gaudemer, J. M. Tonnerre, S. G. Chiuzbăian, C. F. Hague, A. Delmotte, J. M. Dubuisson, G. Cauchon, B. Lagarde, and F. Polack, The SEX-TANTS beamline at SOLEIL: a new facility for elastic, inelastic and coherent scattering of soft x-rays, *J. Phys.: Conf. Ser.* **425**, 072018 (2013).
- [37] S. G. Chiuzbăian, C. F. Hague, A. Avila, R. Delaunay, N. Jaouen, M. Sacchi, F. Polack, M. Thomasset, B. Lagarde, A. Nicolaou, S. Brignolo, C. Baumier, J. Lüning, and J.-M. Mariot, Design and performance of AERHA, a high acceptance

- high resolution soft x-ray spectrometer, *Rev. Sci. Instrum.* **85**, 043108 (2014).
- [38] A. D. Becke, Density-functional thermochemistry. I. The effect of the exchange-only gradient correction, *J. Chem. Phys.* **98**, 5648 (1993).
- [39] C. Lee, W. Yang, and R. G. Parr, *Phys. Rev. B* **37**, 785 (1988).
- [40] M. W. Schmidt Jr. *et al.*, General atomic and molecular electronic structure system, *J. Comput. Chem.* **14**, 1347 (1993).
- [41] R. Krishnan, J. S. Binkley, R. Seeger, and J. A. Pople, Self-consistent molecular orbital methods. XX. A basis set for correlated wave functions, *J. Chem. Phys.* **72**, 650 (1980).
- [42] L. Triguero, O. Plashkevych, L. G. M. Petersson, and H. Ågren, Separate state vs. transition state Kohn-Sham calculations of x-ray photoelectron binding energies and chemical shifts, *J. Electron Spectrosc. Relat. Phenom.* **104**, 195 (1999).
- [43] O. Bunău and Y. Joly, Self-consistent aspects of x-ray absorption calculations, *J. Phys.: Condens. Matter* **21**, 345501 (2009).
- [44] S. A. Guda, A. A. Guda, M. A. Soldatov, K. A. Lomachenko, A. L. Bugaev, C. Lamberti, W. Gawelda, C. Bressler, G. Smolentsev, A. V. Soldatov, and Y. Joly, Optimized finite difference method for the full-potential XANES simulations: Application to molecular adsorption geometries in MOFs and metal-ligand intersystem crossing transients, *J. Chem. Theory Comput.* **11**, 4512 (2015).
- [45] P. R. Amestoy, A. Guermouche, J.-Y. L'Excellent and S. Pralet, Hybrid scheduling for the parallel solution of linear systems, *Parallel Comput.* **32**, 136 (2006).
- [46] U. von Barth and L. Hedin, A local exchange-correlation potential for the spin polarized case, *J. Phys. C: Solid State Phys.* **5**, 1629 (1972).
- [47] A. Girlando, Charge sensitive vibrations and electron-molecular vibration coupling in Bis(ethylenedithio)-tetrathiafulvalene (BEDT-TTF), *J. Phys. Chem. C* **115**, 19371 (2011).
- [48] See Supplemental Material at <http://link.aps.org/supplemental/10.1103/PhysRevB.111.125160> for additional information concerning the samples, the choice of the geometry of the isolated ET molecule used in the calculation, and the results of a tentative calculation of the quasielastic part of the RIXS spectra.
- [49] A. Erba, J. K. Desmarais, S. Casassa, B. Civalleri, L. Donà, I. J. Bush, B. Searle, L. Maschio, L. Edith-Daga, A. Cossard *et al.*, CRYSTAL23: A program for computational solid state physics and chemistry, *J. Chem. Theory Comput.* **19**, 6891 (2023).
- [50] E. Demiralp, S. Dasgupta, and W. A. Goddard III, Electron-transfer boat-vibration mechanism for superconductivity in organic molecules based on BEDT-TTF, *J. Am. Chem. Soc.* **117**, 8154 (1995).
- [51]  $\Gamma = \sqrt{\Gamma_{1s}^2 + \gamma^2}$ .
- [52] J. L. Campbell and T. Papp, Widths of the atomic  $K-N7$  levels, *At. Data Nucl. Data Tables* **77**, 1 (2001).
- [53] L. Ament, M. van Veenendaal, and J. van den Brink, Determining the electron-phonon coupling strength in correlated electron systems from resonant inelastic X-ray scattering, *Europhys. Lett.* **95**, 27008 (2011).
- [54] F. M. F. de Groot, M. W. Haverkort, H. Elnaggar, A. Juhin, K.-J. Zhou and P. Glatzel, Resonant inelastic X-ray scattering, *Nat. Rev. Methods Primers* **4**, 45 (2024).
- [55] S. Moser, S. Fatale, P. Krüger, H. Berger, P. Bugnon, A. Magrez, H. Niwa, J. Miyawaki, Y. Harada, and M. Grioni, Electron-phonon coupling in the bulk of anatase TiO<sub>2</sub> measured by resonant inelastic X-Ray spectroscopy, *Phys. Rev. Lett.* **115**, 096404 (2015).
- [56] S. Fatale, S. Moser, J. Miyawaki, Y. Harada, and M. Grioni, Hybridization and electron-phonon coupling in ferroelectric BaTiO<sub>3</sub> probed by resonant inelastic x-ray scattering, *Phys. Rev. B* **94**, 195131 (2016).
- [57] M. Rossi, R. Arpaia, R. Fumagalli, M. Moretti Sala, D. Betto, K. Kummer, G. M. De Luca, J. van den Brink, M. Salluzzo, N. B. Brookes, L. Braicovich, and G. Ghiringhelli, Experimental determination of momentum-resolved electron-phonon coupling, *Phys. Rev. Lett.* **123**, 027001 (2019).
- [58] A. Kawamoto, Y. Honma, K. I. Kumagai, Electron localization in the strongly correlated organic system  $\kappa$ -(BEDT-TTF)<sub>2</sub>X probed with nuclear magnetic resonance <sup>13</sup>C-NMR, *Phys. Rev. B* **70**, 060510(R) (2004).
- [59] Y. Shimizu, K. Miyagawa, K. Kanoda, M. Maesato, and G. Saito, Emergence of inhomogeneous moments from spin liquid in the triangular-lattice Mott insulator  $\kappa$ -(ET)<sub>2</sub>Cu<sub>2</sub>CN<sub>3</sub>, *Phys. Rev. B* **73**, 140407(R) (2006).
- [60] I. Kimchi, J. P. Sheckelton, T. M. McQueen, and P. Lee, Scaling and data collapse from local moments in frustrated disordered quantum spin systems, *Nat. Commun.* **9**, 4367 (2018).
- [61] M. Matsuura, T. Sasaki, M. Naka, J. Müller, O. Stockert, A. Piovano, N. Yoneyama, and M. Lang, Phonon renormalization effects accompanying the 6 K anomaly in the quantum spin liquid candidate  $\kappa$ -(BEDT-TTF)<sub>2</sub>Cu<sub>2</sub>(CN)<sub>3</sub>, *Phys. Rev. Res.* **4**, L042047 (2022).